PHYSICAL REVIEW B VOLUME 13, NUMBER 12 15 JUNE 1976

High-resolution temperature-dependent inelastic low-energy electron diffraction applied to the surface-plasmon dispersion of aluminum (100)†

J. F. Wendelken*
Coordinated Science Laboratory, University of Illinois, Urbana, Illinois 61801
(Received 11 August 1975)

Elastic and inelastic low-energy-electron-diffraction measurements on a clean Al(100) surface have been obtained with a new high-resolution electron diffractometer. These data, together with data obtained independently at another laboratory, provide the experimental basis for the determination of the surface-plasmon dispersion relation. A survey of specular elastic scattering is used to select elastic resonances which may be described by single scattering theory. Inelastic data are presented which are associated by two-step inelastic scattering with the selected elastic diffraction resonances. The temperature dependence of the inelastic coherent and diffuse scattering is also examined and its effect on the measurement of the surface-plasmon dispersion relation is discussed.

I. INTRODUCTION

With the development in recent years of more sophisticated surface-analysis tools,[1] the discipline of surface physics has emerged as a quantitative science.[2] The development of improved theoretical models has called for more plentiful and more precise data. One such area of recent quantitive improvement involves the understanding of the surface electronic structure as characterized by the surface-plasmon dispersion relation (SPDR).[3] The most convenient approach to measurement of the SPDR utilizes the phenomenon of inelastic low-energy electron diffraction (ILEED).[3-16] ILEED is related to elastic low-energy electron diffraction (ELEED) by virtue of the fact that the characteristic energy-loss processes, such as plasmon creation, involve insufficient momentum transfer to backscatter the electrons.[2] Hence, a two- or more step scattering process must occur which includes an elastic diffraction step. As a result, resonances in the ILEED structure are closely associated with ELEED resonances. Theoretical work has centered on the development of an analytical procedure based on a two-step model of inelastic diffraction for the extraction of the SPDR from inelastic electron scattering intensities.[3,6-8,16] Appropriate experimental work for the measurement of the SPDR has dealt primarily with aluminum which is a nearly-free-electron metal. Burkstrand[9] and Burkstrand and Propst[10] have examined nonspecular elastic and inelastic scattering from Al(100). Specular data which are easier to obtain and utilize have been gathered by Porteus and Faith[11] for Al(111) and an analysis of this was presented by Duke and Landman.[12]

In this paper specular elastic and inelastic low-energy electron scattering from the (100) surface of aluminum is examined. The data were obtained with a new high-resolution ($30 \leq \Delta E < 500$ meV, $\Delta\theta \leq 1°$) scanning low-energy electron diffractometer. Included in the data is a survey of ELEED and a set of ILEED data which have been combined with data of Porteus and Faith[15] and used in a recent measurement of the surface-plasmon dispersion relation for Al(100).[14] The elastic data, which include the first absolute intensity energy-intensity profiles obtained at low temperatures (85 °K), are listed and are available from the author. Also included is an examination of the temperature dependence of diffuse scattering and its effect on the measured plasmon dispersion. Most of the measurements presented here were obtained using a resolution of $\Delta E = 100$ meV. Use of higher resolutions with this instrument is only necessary for such tasks as the measurement of adsorbate vibrational energies which is beyond the scope of this paper and is presented elsewhere.[13]

The remainder of this paper is organized as follows. Section II describes the apparatus, target preparation, and experimental measurements. Section III is devoted to the survey of specular elastic scattering which was a necessary prelude to the measurement of the surface-plasmon dispersion relation. Section IV presents a survey of inelastic data including a look at phonon-assisted inelastic diffraction and Sec. V presents surface-plasmon dispersion data.

II. APPARATUS

In the past, the majority of low-energy-electron-diffraction measurements have been performed with display or scanning-type systems having only moderate energy and angular resolutions ($\Delta E > 0.5$ eV, $\Delta\theta > 2°$). Those systems which have employed deflection analyzers to achieve higher-energy resolutions have heretofore been constrained to operate at fixed angles of incidence and emergence.

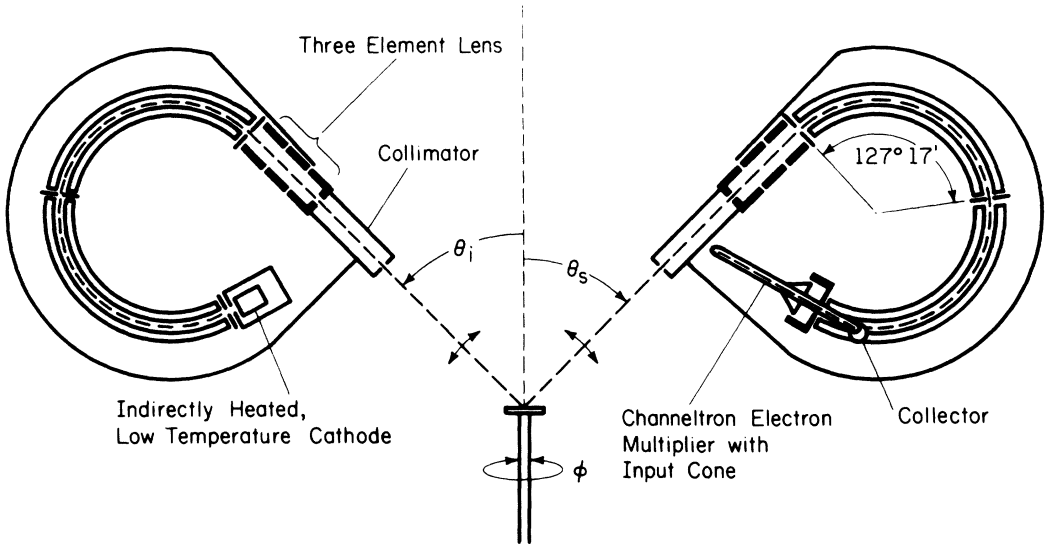

FIG. 1. Schematic of high-resolution low-energy electron diffractometer.

The instrument used for this study is described in detail elsewhere.[13,17] A schematic of the basic instrument is shown in Fig. 1. It possesses an electron monochromator and an energy analyzing electron collector which are capable of providing a net resolution of $\Delta E = 30$ meV and $\Delta\theta = 1°$. Each is constructed with double 127° electrostatic energy selectors and is independently rotatable about a common latitude axis θ. The target is rotatable about the azimuthal axis ϕ which is at right angles to the latitude axis. The monochromator supplies a beam of electrons at the primary energy E_p and incident angle θ_i, and the collector detects those electrons which leave the target with energy E_s and an angle θ_s. The energy which may be lost in the scattering process is defined to be $W = E_p - E_s$. The angles $\theta_i = \theta_s = 0$ are defined to be in the direction normal to the target surface. The angle $\phi = 0$ is defined to be the (10) direction of the surface reciprocal lattice.

A large variety of measurements are possible with this instrument. The variables which may be explored are E_p, E_s, W, θ_i, θ_s, and ϕ. By sweeping one variable at a time a variety of data forms may be obtained. For example, energy-intensity profiles of the LEED beams represent the intensity of scattered electrons as a function of E_p when $W = 0$. Energy-loss profiles represent the intensity as a function of W with all other variables fixed. In addition, the temperature of the target may be controlled over the range 85–800 °K so that temperature dependence may be added to each of the above measurements. For all data reported here, the temperature was within 5 °K of the reported temperature.

The single-crystal Al(100) target was mechanically ground with 1-μm alumina to an accuracy better than 0.1° and electropolished in a perchloric acid solution. The target grinding employed a special jig[13,18] which was mounted on an x-ray diffractometer. *In situ* cleaning was provided by bombardment with 500-eV neon ions followed by annealing at 500 °C. To avoid contamination during sputtering and from surface migration, the target was attached to a pure aluminum block with pure aluminum screws. The complete target preparation procedure is discussed in more detail elsewhere.[13,17,18] Monitoring of the target surface for contamination was achieved with Auger electron spectroscopy

III. SURVEY OF SPECULAR ELASTIC SCATTERING

As a preliminary step to the measurement of the SPDR, it is necessary to select elastic resonances which are well represented by the kinematic (single scattering) approximation for specular diffraction,[14,15]

$$E = \frac{1}{\cos^2\theta}\left[-V_0 + \frac{\hbar^2}{2m}\left(\frac{\pi}{d}\right)^2 n^2\right], \tag{1}$$

where V_0 is the inner potential and d is the layer spacing. This results from the use of a kinematical two-step model[3] for the analysis of the SPDR. For this reason, a survey of specular elastic scattering was conducted and a summary of the results is presented in Fig. 2. Table I lists the energy-intensity profiles which have been published in part elsewhere[13] and which may be obtained from the author. Note that the profiles are for several temperatures and that absolute intensities are available.

The straight lines in Fig. 2 indicate the ex-

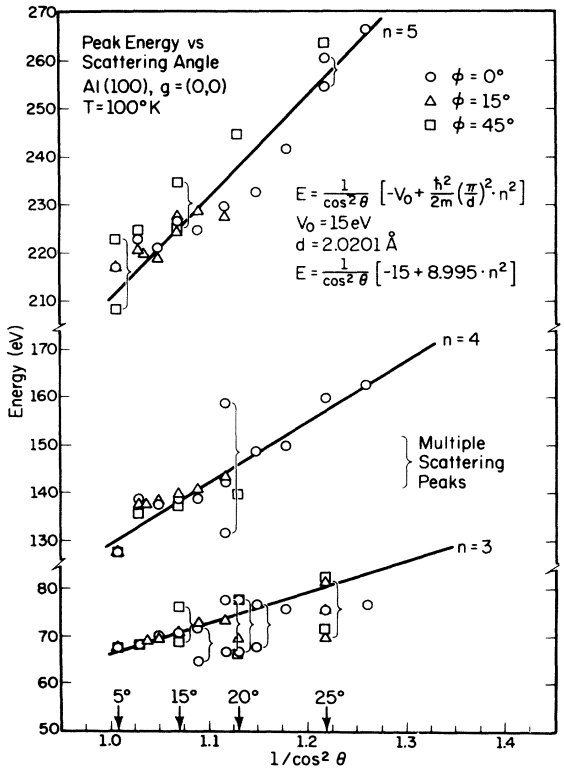

FIG. 2. Comparison of observed specular elastic peak energies to kinematic theory. Groups of multiple scattering peaks illustrate the "Bragg-envelope principle."

pected energy dependence on angle for Bragg resonances in the kinematic approximation. The data points indicate multiple scattering peaks in those cases where distinctly separate peaks occur. The clustering of these multiple scattering peaks about the kinematic position illustrates the "Bragg-envelope principle."[20] A kinematic peak will be defined as one which follows the kinematic line for at least 2° above and below the chosen scattering angle and which is free of obvious multiple scattering peaks over this same range. In order to perform the measurements which are required to determine the surface-plasmon dispersion relation, it is convenient to choose an angle θ which is more than 10° from the normal. The best choices on this basis are the $n = 3$ peaks with coordinates (0°, 15°). The $n = 4$ beam is only marginally acceptable for the coordinates (0°, 15°). The $n = 5$ peak does not appear acceptable in any of the

TABLE I. Specular elastic energy-intensity profiles.

ϕ (deg)	ϕ (deg)	T(°K)	E_p(eV)
5, 10, 15, 20, 25	0, 15, 45	83, 300, 400	30–250
19, 21, 23, 25, 27	0	100	50–250
11, 13, 15, 17, 19	15	100	50–250

cases. These data illustrate the fact that electron scattering from aluminum, a nearly-free-electron metal, is strongly affected by multiple scattering. Despite this, it may still be shown with these data that the surface layer spacing is within 0.1 Å of the bulk layer spacing.[2,13] This is accomplished by the use of averaging techniques[20,21] which reduce the influence of multiple scattering. The rapid change in the peak positions with small angular changes emphasizes the importance of having good angular resolution and accuracy.

IV. SURVEY OF INELASTIC DATA

The discrete energy-loss mechanisms which are typically observed with aluminum may be seen in the energy loss profiles of Fig. 3. Two profiles are shown one profile with a primary energy at the Bragg energy and the other profile with the primary energy at the Bragg energy plus 7 V. At an energy of 1.6 eV a sharp peak occurs which is an interband transition corresponding to the $W_2'W_1$ band gap as calculated by Segall.[22] This peak is very closely associated with the elastic beam direction and is not seen for scattering angles more than 1° from the elastic direction. This interband transition has been seen before in optical experiments at an energy of 1.5 eV and has been seen at an energy of 2.5 eV in a low-resolution electron-scattering experiment.[23] This is the first time that it has been observed at the proper energy by means of electron scattering.

Also seen is a small peak at 6.5 eV. This may

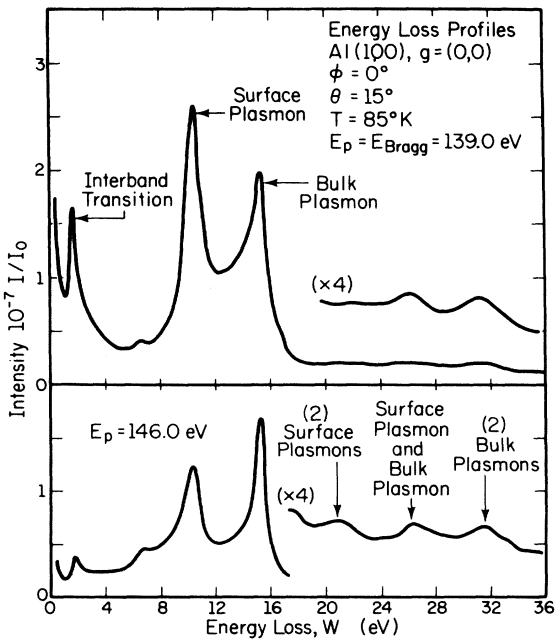

FIG. 3. Typical energy-loss profiles obtained in a specular beam direction.

correspond to the 7-eV peak which was first mistakenly identified as the surface plasmon[24] and which Powell and Swan[25,26] later attributed to the presence of oxygen on the surface. In the present experiment the amount of oxygen on the surface was below the detectable limit of the Auger system.

The surface and bulk plasmons are represented by the peaks near 10 and 15 eV, respectively. Our main attention will be focused on the behavior of these plasmon peaks. Also seen in these energy-loss profiles are peaks which correspond to twice the surface-plasmon energy, twice the bulk-plasmon energy, and the sum of the surface- and bulk-plasmon energies.

The intensity information of Fig. 3 is presented in terms of absolute units so that the cross section for inelastic scattering might be compared to that for elastic scattering. We simply note here that the ratio of the intensity of the surface-plasmon peak with $E_p = 139.0$ eV and $T = 85\,^\circ$K to the intensity of the elastic resonance with the same scattering conditions is 1.6×10^{-4}. The reader must be cautioned to consider the effects of energy and angular resolution when considering this number and comparing it to other experiments. The scattered elastic beam occupies nearly the same energy and angular windows as the incident beam while the inelastic scattering beam is considerably broadened in energy and angle. The analyzer was adjusted to accept energy and angular windows which correspond closely to the elastic beam.

Figure 4 contains a set of energy-loss profiles

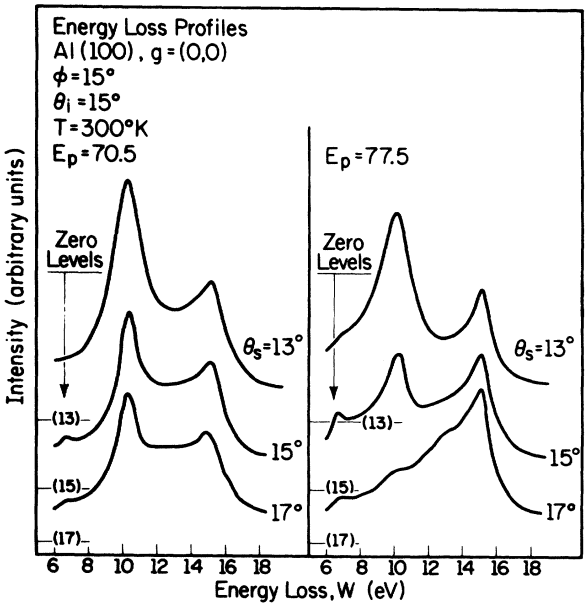

FIG. 4. Energy-loss profiles with $E_P = E_{\text{Bragg}}$ and $E_P = E_{\text{Bragg}} + 7$ eV and $\theta = \theta_{\text{specular}} \pm 2°$.

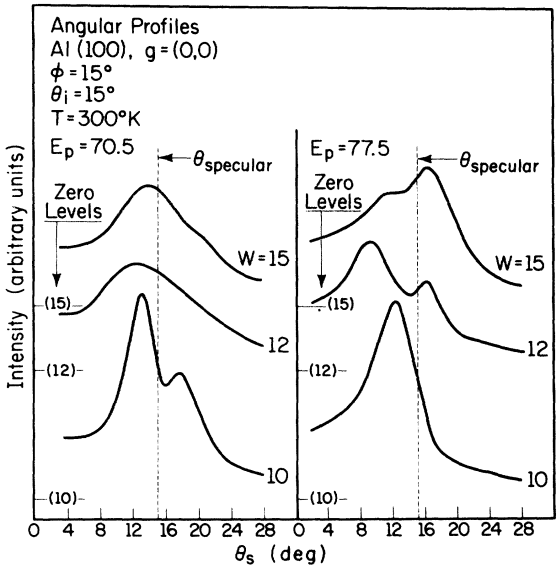

FIG. 5. Inelastic angular profiles with $E_p = E_{\text{Bragg}}$ and $E_P = E_{\text{Bragg}} + 7$ eV and $W = 10$, 12, and 15 eV.

which illustrates the behavior of the surface and bulk plasmons with respect to primary energy and scattering angle. The general behavior displayed here is consistent with the nonspecular inelastic Al(100) data of Burkstrand.[9,10] The plasmon losses are shown for $E_p = E_{\text{Bragg}}$ on the left-hand side and for $E_p = E_{\text{Bragg}} + 7$ eV on the right-hand side. The three scattering angles shown are in the specular direction and 2° above and below the specular direction. A pronounced decrease in the surface-plasmon intensity is seen at the subspecular angle for the higher primary energy. There is also an additional peak which appears at about 13 eV for the lower-right profile. Similar near-specular peaks have been reported by Porteus and Faith.[15] They attributed the near-specular extra peaks to one-electron-type excitations because of the very small momentum which is involved. They also argue against dynamical effects as the cause with the observation that these peaks are suppressed at higher primary energies. The same effect is seen in the present data.

Figure 5 further illustrates the complexity of the inelastic scattering. This series of angular profiles is taken with the same set of scattering conditions as was used for Fig. 4. The specular elastic angular profile is not shown, but is centered about the dotted line and is about 1° wide. These inelastic profiles are on the order of 10° wide, emphasizing the necessity of relating instrumental angular resolution to measured absolute intensities. A qualitative understanding of these angular profiles may be obtained by consideration of energy and momentum conservation,

even though inelastic angular profiles have been shown to be strongly affected by dynamical scattering.[3] Momentum parallel to the surface is conserved when the scattering involves a two-dimensional surface. Given an equal probability for the loss event to contribute a momentum component parallel to the surface $p_{\parallel}$ in any direction, the resulting angular profile will not be symmetric about the elastic beam direction unless the elastic beam emerges normal to the surface. The projection of $\pm p_{\parallel}$ on the curved secondary energy sphere on an Ewald construction as in Fig. 6 of Ref. 13 shows that the angular profile should be shifted slightly away from the normal. In Fig. 5, where the specular scattering angle is 15°, a shift of about 0.5° can be seen in the profile with $E_p = 70.5$ eV and $W = 10$ eV. Only the $w = 10$ eV profiles will be considered because they represent a surface excitation in which case the momentum transfer is parallel to the surface.

As discussed elsewhere[2,27] the small momentum transfer involved in these discrete energy-loss processes is insufficient for backscattering. Therefore, two-step diffraction must be considered in which the loss event is preceded by elastic diffraction (DL) or followed by elastic diffraction (LD). Elastic diffraction, as Fig. 2 shows, displays all the complications of multiple scattering from a three-dimensional lattice. When a DL event occurs, the diffraction event will be strong in the specular direction if the primary energy is equal to the Bragg or other resonance energy. The angular profile after the loss event would then show two peaks, one on either side of the elastic beam direction. If the surface-plasmon creation has equal probability for momentum transfer in any direction parallel to the surface, then the two peaks should be nearly equal in intensity. When an LD process occurs, then the incident beam is first split in two directions in the scattering plane in addition to the associated energy loss. These beams are then diffracted under different conditions. Figure 2 shows that the peak energies generally become smaller as the angle θ is reduced. Thus the diffracted beam which has the smaller angle θ is likely to be closer to a resonant condition for the conditions shown in Fig. 5 with $W = 10$ eV. In the case with $E_p = 77.5$ eV $= E_{\text{Bragg}} + 7$ eV, the DL process is not strong and the LD process associated with the smaller angle θ corresponds almost exactly to the Bragg condition. This explains the suppression of the surface plasmon in the lower right profile of Fig. 4.

Figures 4 and 5 again emphasize the importance of instrumental resolution since small changes in scattering parameters lead to dramatic changes in the profiles. The angular profiles also show that the inelastic diffuse background is not a strong function of the loss energy, but is a strong function of angle in the vicinity of the plasmon peaks. This result has been shown before by Duke and Landman[12] using data from Porteus and Faith.[11] We suggest below though, that there is some dependence of the diffuse background on energy loss and that this is an important consideration when measurements of the plasmon dispersion are made.

To gain insight into the nature of the diffuse background and its effect on the observation of the surface-plasmon dispersion, we examine the temperature dependence of coherent and diffuse inelastic scattering. The incoherent background is caused by both thermal diffuse scattering and surface morphology effects. It is shown elsewhere[13,19] at least insofar as this particular aluminum crystal is concerned that the primary source of the incoherent background in the elastic scattering case is thermal diffuse scattering. In that study it is assumed that the morphological diffuse scattering is independent of temperature and that the thermal diffuse scattering temperature dependence is given by the first term of the expression[21]

$$I = Nf^2(1 - e^{-2M}) + I_0 e^{-2M}, \tag{2}$$

where

$$M = 8\pi^2/\lambda^2 \cos^2\theta \langle \mu^2 \rangle \tag{3}$$

and the mean square atomic displacement is

$$\langle \mu^2 \rangle = \frac{3\hbar^2 T}{m k_B \Theta_D^2}. \tag{4}$$

In this kinematic scattering vibrating lattice model the second term represents the coherent scattering. The Debye-Waller factor is given by e^{-2M} and is determined from the slope of $\ln(I_{\text{coherent}})$ vs T (Debye plot). The temperature dependence observed for any beam condition represents a mixture of surface and bulk properties; hence the Debye temperature which is used to characterize the temperature dependence is generally written as an effective temperature, Θ_D^{eff}. The temperature dependence of coherent elastic scattering from Al(100) has been examined elsewhere.[13,19,29]

Figure 6 shows three angular profiles taken with a loss energy of 10.0 eV with temperature the variable. The primary energies are adjusted as required to allow for the thermal lattice expansion. We should expect the temperature dependence of the inelastic profiles to be at least qualitatively the same as for the elastic profiles as a result of the inclusion of an elastic scattering event in the inelastic scattering process. The intensity of the coherent scattering decreases as the temperature is increased while the incoherent background increases. This is the effect expected

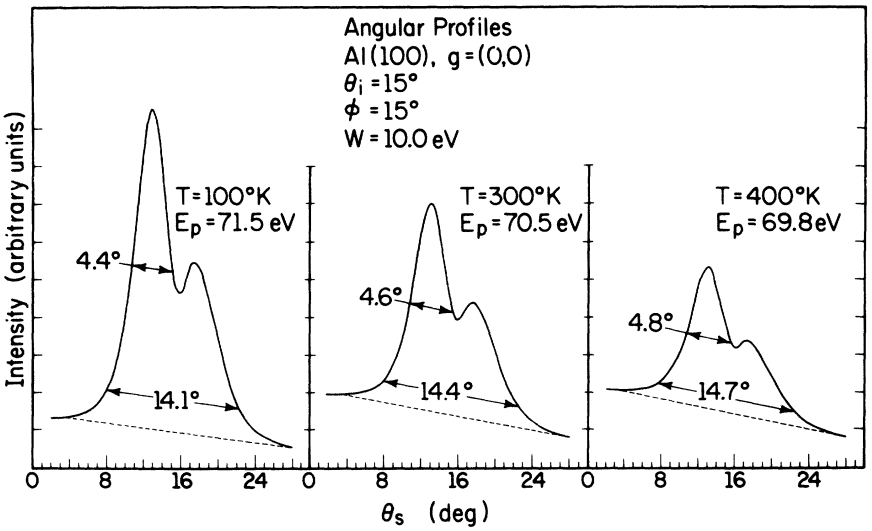

FIG. 6. Temperature dependence of inelastic angular profiles with W = 10 eV. The primary energy is the Bragg energy adjusted at each temperature for thermal lattice expansion.

from multiple Debye phonon losses.[3,28] The peaks also appear to broaden slightly as the temperature is increased which is the result of single Debye phonon losses.[3,28]

The temperature dependence of both bulk and surface-plasmon peaks may be plotted on Debye plots as is done with elastic resonances. The temperature dependence observed is then representative in part of the elastic resonances involved in the two-step scattering. Although a careful series of measurements was not made for this purpose in the present work, it was obvious that the bulk plasmon displays a higher Θ_D^{eff} than the surface plasmon. Thus, as expected the scattering events associated with the bulk plasmon occur deeper in the bulk than with the surface plasmon case. It has been generally accepted that the surface layer has a lower Θ_D^{eff} which means that the thermal vibration amplitude of the surface atoms is greater than that of the bulk atoms.[16]

The temperature dependence of the diffuse scattering is more difficult to define exactly because the coherent scattering displays a larger angular spread and is not easily separated from the incoherent scattering. The dotted lines in Fig. 6 are not an indication of the incoherent scattering, but merely a convenient baseline. In order to estimate the amount of diffuse scattering at an angle, say $\theta_s = 5°$, we need to make two assumptions. First, it is reasonable to expect that the incoherent scattering is primarily thermal diffuse scattering as in the elastic case. Second, we need to assume that the Debye-Waller factor e^{-2M}, determined from the coherent inelastic peaks, may be applied to the incoherent scattering as in the elastic case. At the angle $\theta_s = 5°$ for the 70 eV elastic beam, the morphological diffuse scattering was shown to be about 10% of the total diffuse scattering at a temperature of 300 °K.[13,19] Using Eq. 1, we then write expressions for the total intensity at $\theta_s = 5°$ for two temperatures T = 100 and 300 °K. Solving this set of equations then shows that the ratio of coherent to diffuse intensity at T = 300 °K is about 0.34 and at T = 100 °K is about 1.20. Thus, diffuse scattering is clearly dominant at an angle of 10° from the specular direction for a temperature of 300 °K and above.

V. SURFACE-PLASMON DISPERSION MEASUREMENTS

In the remainder of this paper we present data used for a measurement of the SPDR for Al(100). The determination via a kinematical two-step model of the SPDR from this data and from data of Porteus and Faith[15] is presented elsewhere by Duke *et al.*[14] The initial step in the analysis of the SPDR is the selection of data. In order to use a kinematical two-step model, particularly in the case of an LD resonance,[14] it is necessary to select ELEED resonances (E, θ, ϕ) which are nearly kinematic in their behavior. The ILEED resonances which are associated with these ELEED resonances by the two-step ILEED process are then studied. For this study we have chosen the following ELEED resonances which we label as beams No. 1, No. 2, and No. 3.

Beam No. 1: $\phi = 15°$, $\theta = 15°$, $E_p = 140$ eV;

Beam No. 2: $\phi = 15°$, $\theta = 15°$, $E_p = 70$ eV;

Beam No. 3: $\phi = 0°$, $\theta = 15°$, $E_p = 140$ eV.

Having chosen the ELEED resonances with which to work, the first step of the analysis is completed

by parameterizing each ELEED resonance in terms of kinematic theory to determine the inner potential V_0 and inelastic collision damping length, λ_{ee}.[3] For beam No. 2, the best fit of kinematic theory with the peak position and shape is obtained[30] when $V_0 = 17.7$ eV and $\lambda_{ee} = 7.5$ Å. These parameters are subsequently used when the two-step analysis is applied to the ILEED data associated with this particular ELEED resonance.

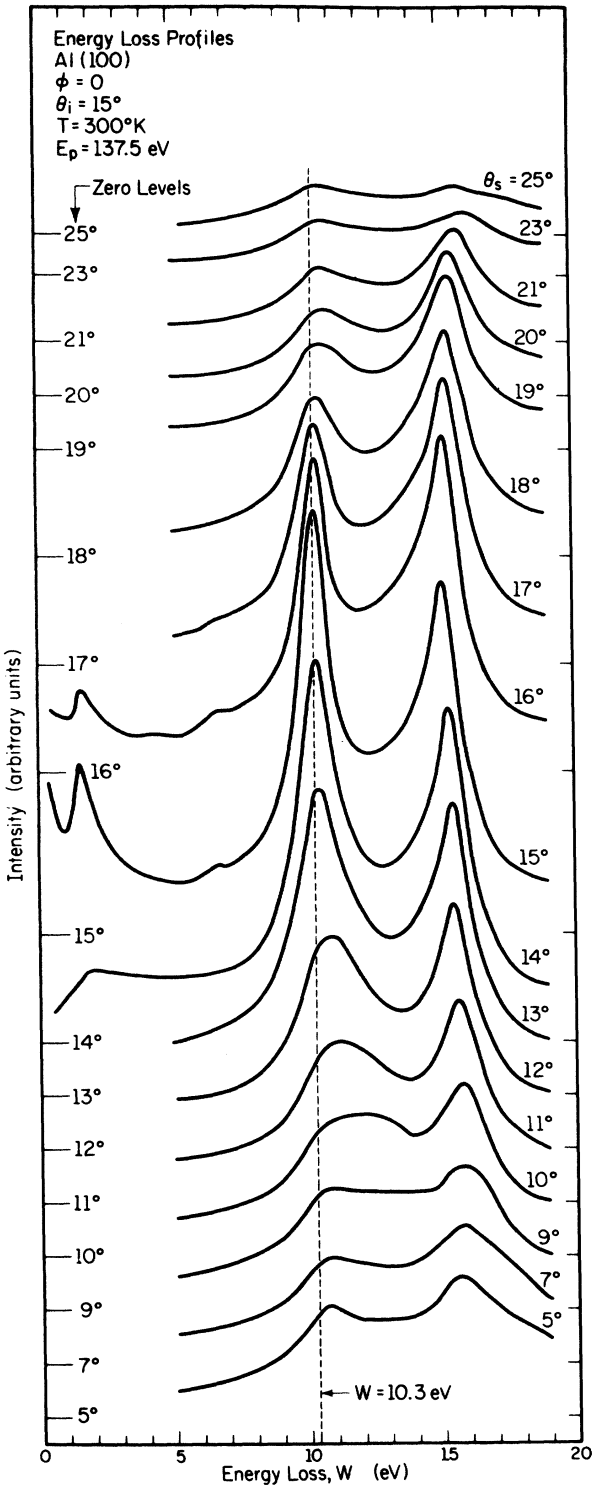

FIG. 7. Energy-loss profiles associated with beam No. 1 which are used to measure surface-plasmon dispersion.

Duke and Landman[3] have shown that energy-loss profiles are the most suitable form of inelastic data to be used with a two-step model. By observing the energy-loss profiles in a series of off-specular directions, a momentum transfer may be associated with a given energy loss. In this work, energy-loss profiles were taken at angular intervals of 1° over the range $\theta_s = \theta_{\text{specular}} \pm 6°$ and in intervals of 2° over the range $\theta_s = \theta_{\text{specular}} \pm 15°$. The data were obtained at two temperatures $T = 100$ °K and $T = 300$ °K. Figure 7 displays the profiles which are associated with beam No. 3 over a range 10° above and below the specular direction with $T = 300$ °K. The motion of the surface-plasmon peak as well as the bulk-plasmon peak can be easily seen as a function of angle. The surface plasmon occurs at an energy of 10.3 eV in the specular direction which is the case involving nearly zero momentum transfer. The maximum energy shift occurs for $\theta = 10°$. The peak in this case is centered at about 11.5 eV, however, the peak is quite broad and precise measurement is difficult. In these profiles the 1.6 eV interband transition loss and the 6.5 eV loss are also evident. Both losses display very little divergence from the elastic beam direction, which indicates that both are associated with one-electron-type excitations.

The dispersion characteristics observed with the three beams are summarized in Fig. 8. In the top three panels, the surface-plasmon peak intensity is shown as a function of θ_s. The specular direction in all three cases occurs for $\theta_s = 15°$ and the loss energy associated with each point is the loss energy observed at each angle. In the bottom two rows of panels is shown the loss energy measured as a function of θ_s at temperatures of 300 and 100 °K. The error bars indicate the uncertainty in the measurements of a given peak position which is indicative of the peak width. The angular dependence of this peak width is an indication of the angular dependence of the plasmon damping Γ.[3,14] The most interesting initial observation is that data for $T = 100$ °K for all three cases indicate a greater dispersion for the low-temperature case. The plasmon damping also appears to depend in some indefinite way on the temperature. The apparent asymmetry of the dispersion data about the $p_{\parallel} = 0$ direction has been attributed in part to the overlap of the bulk-plasmon loss peak.[15] However, with the data presented in Fig. 7, this does not appear to be an

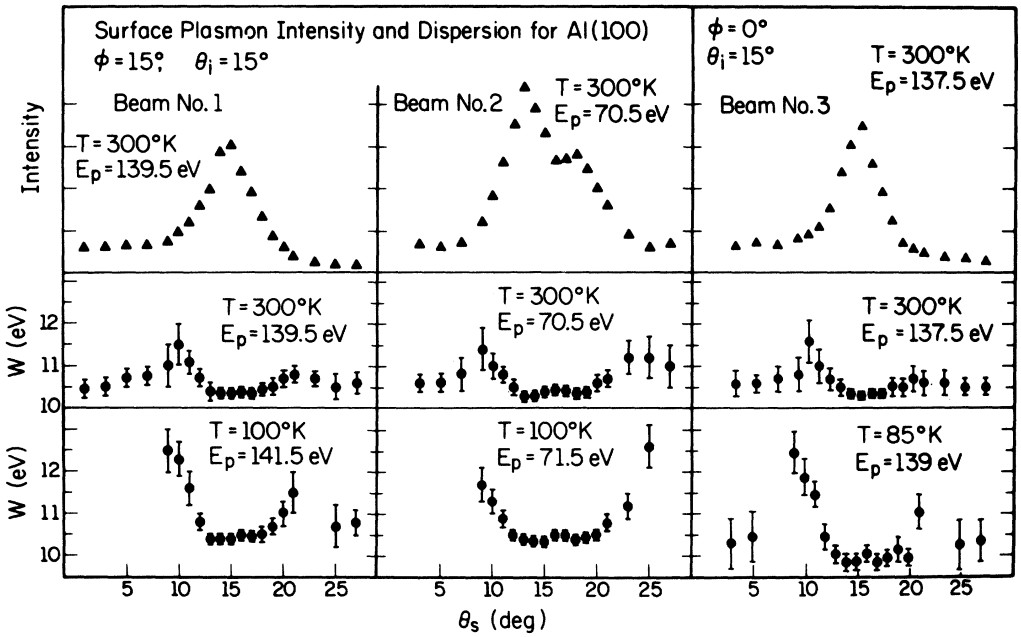

FIG. 8. Surface-plasmon intensity and dispersion data from beams Nos. 1, 2, and 3.

adequate explanation. The explanation may be found in the two-step model[8,15] though it has not been verified in this case.

Three factors combine to create the apparent temperature dependence of the dispersion. First, it is evident from Fig. 6 and the discussion in Sec. IV that for angles greater than 6° from the specular direction, the intensity observed is primarily due to the thermal diffuse background. If it is noted that for the $\theta_s = 5°$ profile in Fig. 7 the diffuse scattering accounts for roughly three fourths of the total intensity as discussed in Sec. IV, then it is obvious that the diffuse background must exhibit a slight energy dependence over the range of interest $W = 9-12$ eV. The inelastic diffuse scattering is associated with elastic diffuse scattering by the two-step process as in the case of coherent scattering. A random direction will be associated with the elastic scattering event. The loss energy observed is then weighted toward the most probable loss energy which is shown by Fig. 8 to be the near zero momentum loss energy. This background can thus cause a distortion in the relatively weak loss profiles which occur in the vicinity of 5° above or below the specular direction. The peaks may be shifted and/or broadened. Thus, loss energies measured at the extreme angles are representative of the diffuse background as well as the plasmon dispersion. At low temperatures the diffuse scattering is considerably reduced so that the distortion of the loss profiles will be reduced. It is therefore desirable to cool targets to a temperature at which the thermal diffuse scattering is minimized to reduce this distortion. Reduction of the morphological diffuse scattering is a separate and more difficult question which has not been explored.

The second factor in the temperature dependence of the dispersion involves the angular resolution of the system. Consider the case where $\theta = 10°$. If the instrument has a poor angular resolution, say 10°, the instrument will see electrons arriving in the angular window between 5° and 15°. Obviously, there is a greater intensity of electrons which represent the surface plasmon toward the 15° position. Therefore, the loss profile will be distorted toward the energy which occurs for $\theta_s = 15°$. With a resolution of 1° the energy of the peaks will be more faithfully represented. Now, as the temperature is decreased, the angular profiles have been seen to narrow as in Fig. 6. Single phonon broadening[3] of elastically diffracted electron beams is the same order of magnitude. Reducing the temperature has the same effect as improving the instrumental angular resolution. It is apparent from this that the most accurate measurement of the SPDR should be obtained from high-resolution low-temperature measurements.

A third possible factor is the change in electron density as a function of temperature. The near zero momentum plasmon energy is proportional to the square root of the electron density in the free-electron model.[31] If the surface layer is assumed to possess the same thermal expansion coefficient as the bulk, then the energy of the plasmon would increase about 0.07 eV when the

temperature is reduced from 300 to 100 °K. Dasgupta, Kumar, and Beck[32] recently derived a semiclassical integral expression for the SPDR which indicates a dependence on the surface electron density profile. In order to compare data to this theory, it will first be necessary to carefully account for the other effects. Alternatively, by examining the SPDR behavior for a material which reorders its surface as a function of temperature, a phase change should also be seen in the SPDR. Evidence for this is the difference in the SPDR which has now been observed for two crystallographic faces of aluminum.[14,15]

Consideration of the relative magnitude of these effects indicates that subtraction of the diffuse background from higher-temperature data is the primary solution to the problem. A shift in the angular resolution from 1° to 2° will shift the loss energy by 0.1 eV at the most. In the data for beam No. 1 at an angle $\theta_s = 11°$, the loss energy observed is 11.1 eV when $T = 300$ °K. For $T = 100$ °K the loss energy is 11.6 eV. At this position, it appears from the top panel that the total intensity is approximately one half diffuse and one half coherent. A simple average of the low-temperature loss energy and the loss energy in the diffuse scattering peak which is approximately 10.5 eV according to the $\theta_s = 5°$ profile of Fig. 7, is approximately equal to the loss energy observed for $T = 300$ °K.

In the analysis of the 300 °K data by Duke *et al.*,[14] the second step of the procedure is the subtraction of a calculated diffuse background from the inelastic data. The diffuse background calculation was based on a series of angular profiles at various loss energies. The form of the diffuse background obtained from this had the energy independent form[14]

$$\left(\frac{d\sigma}{d\Omega\, dE}\right)_{\text{incoh}} = 0.05 + \frac{0.017}{\theta' + 0.01}, \qquad (5)$$

where θ is the scattered angle measured from the target normal. In order to minimize the effects of the distortions discussed above, the data used for calculation of the surface-plasmon dispersion were limited to loss profiles in an angular range such that the intensities were primarily due to coherent scattering. The uncertainties which arise from this are one of the reasons why the plasmon dispersion relations which have been obtained contain sizeable ambiguities. The SPDR which has been obtained in association with the present work is given by[14]

$$\hbar\omega_s(p_{\parallel}) = 10.4(\pm 0.1) - 2(\pm 1)p_{\parallel} + 9(\pm 3)p_{\parallel}^2 . \qquad (6)$$

The energy $\hbar\omega_s$ is in eV and the momentum parallel to the surface $p_{\parallel}$ is in Å^{-1}. By means of a more detailed study of the temperature dependence of coherent and diffuse inelastic scattering, it should be possible to expand the range of useful data and thus to reduce these uncertainties.

VI. CONCLUSIONS

We have presented elastic and inelastic electron diffraction data obtained from an Al(100) target in a high-resolution low-energy electron diffractometer. The elastic data have been used to define kinematiclike elastic scattering resonances. Inelastic energy-loss profiles and angular profiles associated with selected elastic resonances were obtained to provide the basis for a measurement of the surface-plasmon dispersion relation. An apparent temperature dependence in the raw plasmon dispersion data has been shown to be primarily the result of the temperature dependence of the inelastic thermal diffuse background. As a consequence of the high energy and angular resolution of the system, it was also possible to observe clearly an interband transition loss of 1.6 eV and to show the sensitivity of inelastic scattering and multiple elastic scattering to energy and angle.

ACKNOWLEDGMENTS

The author is indebted to Dr. C. B. Duke for many helpful discussions during the course of this work, and to Dr. F. M. Propst who introduced the author to surface physics and served as his thesis advisor, and to the staff of the Coordinated Science Laboratory who made it possible to construct and use the electron diffractometer.

---

†This work was supported in part by the Joint Services Electronics Program (U. S. Army, U. S. Navy, and U. S. Air Force) under Contract DAAB 07-72-C-0259.

*Present address: Oak Ridge National Laboratory, Oak Ridge, Tenn. 37830.

[1]C. B. Duke and R. L. Park, Phys. Today 25, 23 (1972).
[2]C. B. Duke, Jpn. J. Appl. Phys. 13, (1974).
[3]C. B. Duke and U. Landman, Phys. Rev. B 7, 1368 (1973).
[4]C. B. Duke and G. E. Laramore, Phys. Rev. B 3, 3183 (1971).
[5]G. E. Laramore and C. B. Duke, Phys. Rev. B 3, 3198 (1971).
[6]A. Bagchi, C. B. Duke, P. J. Feibelman, and J. O. Porteus, Phys. Rev. Lett. 27, 998 (1971).
[7]C. B. Duke and A. Bagchi, J. Vac. Sci. Technol. 9, 738 (1972).
[8]A. Bagchi and C. B. Duke, Phys. Rev. B 5, 2784 (1972).
[9]J. M. Burkstrand, Ph. D. thesis (University of Illinois, 1972) (unpublished); and Phys. Rev. B 7, 3443 (1973).
[10]J. M. Burkstrand and F. M. Propst, J. Vac. Sci.

Technol. 9, 731 (1972).
[11]J. O. Porteus and W. N. Faith, Phys. Rev. B 8, 491 (1973).
[12]C. B. Duke and U. Landman, Phys. Rev. B 8, 491 (1973).
[13]J. F. Wendelken, Ph. D. thesis (University of Illinois, 1975) (unpublished); Coordinated Science Laboratory Report No. R-667 (unpublished).
[14]C. B. Duke, L. Pietronero, J. O. Porteus, and J. F. Wendelken, Phys. Rev. B (to be published).
[15]J. O. Porteus and W. N. Faith, Phys. Rev. B (to be published).
[16]C. B. Duke, Adv. Chem. Phys. 27, 1 (1974).
[17]J. F. Wendelken and F. M. Propst (unpublished).
[18]J. F. Wendelken, S. P. Withrow, and C. Foster (unpublished).
[19]J. F. Wendelken (unpublished).
[20]C. W. Tucker, Jr. and C. B. Duke, Surf. Sci. 29, 237 (1972).
[21]M. G. Lagally, T. C. Ngoc, and M. B. Webb, Phys. Rev. Lett. 26, 1557 (1971).
[22]B. Segall, Phys. Rev. 124, 1797 (1961).
[23]L. H. Jenkins and M. F. Chung, Surf. Sci. 31, 180 (1972).
[24]O. Klemperer and J. P. Shepherd, Adv. Phys. 12, 355 (1963).
[25]C. Powell and J. Swan, Phys. Rev. 115, 869 (1959).
[26]C. Powell and J. Swan, Phys. Rev. 118, 640 (1960).
[27]C. B. Duke, and U. Landman, Phys. Rev. B 6, 2956, 2968 (1972).
[28]R. F. Barnes, M. G. Lagally, and M. B. Webb, Phys. Rev. 171, 627 (1968).
[29]D. T. Quinto, B. W. Holland, and W. D. Robertson, Surf. Sci. 32, 139 (1973).
[30]C. B. Duke (private communication).
[31]D. Bohm and D. Pines, Phys. Rev. 92, 609 (1955).
[32]B. B. Dasgupta, P. Kumar, and D. E. Beck, Surf. Sci. 48, 241 (1975).